

Perimeter Governed Minority Carrier Lifetimes in 4H-SiC p⁺n Diodes Measured by Reverse Recovery Switching Transient Analysis

Philip G. Neudeck

NASA Lewis Research Center, 21000 Brookpark Rd., M.S. 77-1
Cleveland, OH 44135

Abstract

Minority carrier lifetimes in epitaxial 4H-SiC p⁺n junction diodes were measured via an analysis of reverse recovery switching characteristics. Behavior of reverse recovery storage time (t_s) as a function of initial ON-state forward current (I_F) and OFF-state reverse current (I_R) followed well-documented trends which have been observed for decades in silicon p⁺n rectifiers. Average minority carrier (hole) lifetimes (τ_p) calculated from plots of t_s vs. I_R/I_F strongly decreased with decreasing device area. Bulk and perimeter components of average hole lifetimes were separated by plotting $1/\tau_p$ as a function of device perimeter-to-area ratio (P/A). This plot reveals that perimeter recombination is dominant in these devices, whose areas are all less than 1 mm². The bulk minority carrier (hole) lifetime extracted from the $1/\tau_p$ vs. P/A plot is approximately 0.7 μ s, well above the 60 ns to 300 ns average lifetimes obtained when perimeter recombination effects are ignored in the analysis. Given the fact that there has been little previous investigation of bipolar diode and transistor performance as a function of perimeter-to-area ratio, this work raises the possibility that perimeter recombination may be partly responsible for poor effective minority carrier lifetimes and limited performance obtained in many previous SiC bipolar junction devices.

Key Words: 4H-SiC, p-n junctions, rectifiers, bipolar junction devices, minority carrier lifetime, surface recombination, reverse recovery

Introduction

Silicon carbide's demonstrated ability to function under extreme high-power and/or high-temperature operating conditions is expected to enable significant improvements to a far-ranging variety of systems. These range from improved high-voltage switching for energy savings in electric power distribution and electric vehicles to more powerful microwave electronics for radar and communications to sensors and controls for cleaner-burning, more fuel-efficient jet aircraft and automobile engines. Both unipolar and bipolar SiC device electronics are being developed worldwide to meet the specific needs of various applications¹.

In the case of bipolar devices, the recombination lifetime of minority carriers injected across pn junctions plays a key role in determining device performance, as bipolar gain, maximum current rating, and maximum operating frequency are inherent functions of minority carrier lifetime²⁻⁴. As in the case of silicon bipolar electronics, the ability to control SiC minority carrier lifetimes to be short (nanoseconds) or long (many microseconds) as desired would permit application-specific optimization of SiC bipolar device characteristics. In some

applications shorter minority carrier lifetimes facilitate fast carrier recombination required to realize high-frequency bipolar device switching, while longer lifetimes that maximize bipolar device current density and gain (at the tradeoff expense of device switching speed) are often desired in lower-frequency applications.

Most prototype bipolar electrical devices reported in SiC have exhibited low effective minority carrier lifetimes on the order of nanoseconds. While beneficial for demonstrating high switching speeds, these short effective lifetimes limit experimental bipolar device current densities and gains. For example, the maximum current gain reported at room temperature in SiC bipolar junction transistors to date is 15 (with an extracted lifetime of approximately 5 ns), which is insufficient for many circuit applications⁵. While variations in material sources and doping and characterization methods make valid comparisons of lifetime data somewhat problematic, minority carrier lifetimes ascertained by optical methods on unprocessed SiC epitaxial material appear to be significantly longer (ranging from 0.1 μ s to 2.1 μ s)⁶ than average lifetimes measured in actual SiC bipolar diodes and transistors (2 ns to 0.1 μ s)^{5, 7}. Even the work of Kordina et. al.^{6, 8}, in which low-doped epilayers were optically characterized and then subsequently employed in pn junction diode fabrication, noted a significant inconsistency between the experimentally obtained electrical device performance and the theoretically modeled performance obtained by plugging the optically-measured lifetimes into device simulations.

Improvement of the minority carrier lifetimes in operational SiC devices is important if SiC bipolar electronics are to be implemented and utilized to their full potential. It is therefore important to understand the physical mechanisms limiting minority carrier lifetimes in prototype SiC bipolar devices, so that appropriate processing changes to SiC device fabrication might be implemented to bring device minority carrier lifetimes up to the same level as optically measured lifetimes on unprocessed SiC epitaxial material.

This paper presents experimental evidence that perimeter-governed surface recombination may be a significant contributing mechanism to poor effective minority carrier lifetimes observed in prototype SiC bipolar junction devices. In particular, the effective minority carrier lifetimes of one lot of 4H-SiC p⁺n junction diodes (as measured by reverse recovery transient analysis) are shown to be dominated by surface recombination occurring around the diode periphery, instead of recombination occurring at bulk recombination centers in the SiC epitaxial junction material. The magnitude of the perimeter-induced decrease in effective lifetime observed in this work was large enough to account for many discrepancies between optically measured minority carrier lifetime data and minority carrier lifetimes extracted from device electrical performance.

Experimental

The homoepitaxial p⁺n junction diode structure shown in Fig. 1 was grown by NASA Lewis on a 4H-SiC substrate polished at a 3.5° tilt angle off the (0001) silicon face purchased from

Cree Research⁹ using previously described chemical vapor deposition procedures¹⁰. Prior to device definition processing a course backside wafer polish was carried out to remove part of the polycrystalline SiC material deposited onto the wafer backside during epitaxy. Following liftoff patterning of an aluminum etch mask, device mesas were defined to a depth of 2 μm by Reactive Ion Etching in 90% CHF_3 : 10% O_2 at 400 W rf power with a chamber pressure of 150 mTorr. The aluminum etch mask was stripped and E-beam deposited gold was subsequently liftoff patterned to form unannealed ohmic contacts to the degenerately doped p^+ cap epilayer. Gold metallization was also deposited on the wafer backside to form the substrate contact. No surface passivation processing (such as thermal oxidation or insulator deposition) was employed in this work. Initial electrical characterization was carried out on a probing station. Capacitance-voltage profiling indicated the n-layer carrier concentration varied between 2 to 4 $\times 10^{16} \text{ cm}^{-3}$ across the majority of the wafer. Individual die were then sawed-apart and mounted with conductive epoxy into TO-39 packages for wire bonding. Prior to being placed into the pulse-test circuit, the I-V and C-V characteristics of packaged devices were re-verified. All electrical measurements were carried out at an ambient temperature of 297 K.

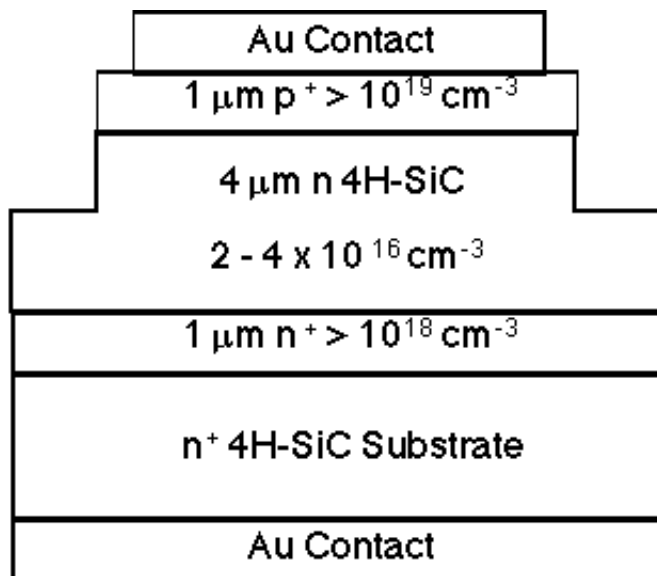


Fig. 1. 4H-SiC p^+n diode cross-section. No intentional surface passivation was employed in these devices.

When a pn junction semiconductor diode is rapidly switched from forward into reverse bias, excess minority carriers remaining from forward bias injection must recombine before current flow through the diode can drop to near-zero^{2, 4, 11}. As discussed in Ref. 2, this gives rise to the idealized (zero inductance) reverse recovery switching transient depicted in Fig. 2 for a p^+n diode. The storage time t_s as defined in Fig. 2 is directly related to the average minority (hole) carrier lifetime τ_p by²:

$$t_s = \tau_p \left\{ \operatorname{erf}^{-1} \left[1 + \frac{1}{I_R / I_F} \right] \right\}^2 \quad (1)$$

where I_F is the forward current flowing through the diode just prior to switching ($t = 0^-$) and I_R is the constant reverse recovery current flowing during the storage phase which occurs between time $t = 0^+$ and $t = t_s$. Diode current flow then drops off quasi-exponentially to near zero during the subsequent recovery phase which occurs between $t = t_s$ and $t = t_{rr}$ where t_{rr} is the reverse recovery time often listed in diode specification sheets.

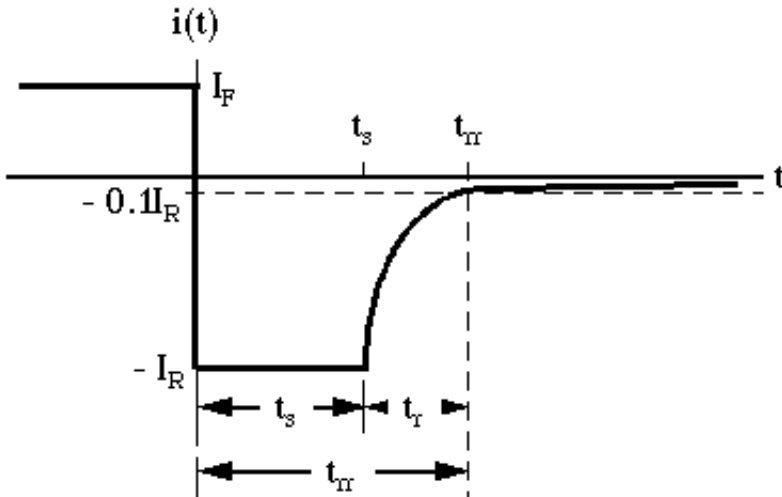


Fig. 2. Idealized (zero-inductance) current response of p^+n junction diode when instantaneously switched from forward current I_F to reverse bias at $t = 0$. Significant reverse recovery current flows until excess minority charge in junction recombines. The storage time t_s and reverse recovery time t_{rr} are functions of minority carrier lifetime. After Ref. 2.

The effective minority carrier lifetimes were characterized by measuring the reverse recovery switching transient properties of each diode in a minimum inductance test circuit. Reverse recovery testing was carried out using the charge line circuit depicted in Fig. 3. This circuit nominally stressed the device under test using manually triggered single-shot rectangular shaped pulses of 200 ns width. The pulse voltage amplitude was controlled by adjusting the high-voltage DC (HVDC) supply, which charged a 1/2-inch diameter 150-ft semirigid coax transmission line. The fast-risetime pulse is formed by the discharge of the semirigid coax when the mercury vapor switch is momentarily triggered. The diode is initially forward biased by the DC supply through the 200 ohm (or 400 ohm) resistor. A 10 μ F high-voltage capacitor isolates the initial DC bias from the transmission line circuit, but permits the fast-risetime pulse to rapidly switch the diode under test from forward bias into reverse bias. The Tektronix CT2/P6041 current probe/transformer monitors the transient reverse recovery current of the diode over the frequency range from 1 kHz to 500 MHz. Prior to testing SiC-based diodes, circuit functionality and was verified by measuring the reverse recovery characteristics of several known silicon diodes with near 1 μ s lifetimes.

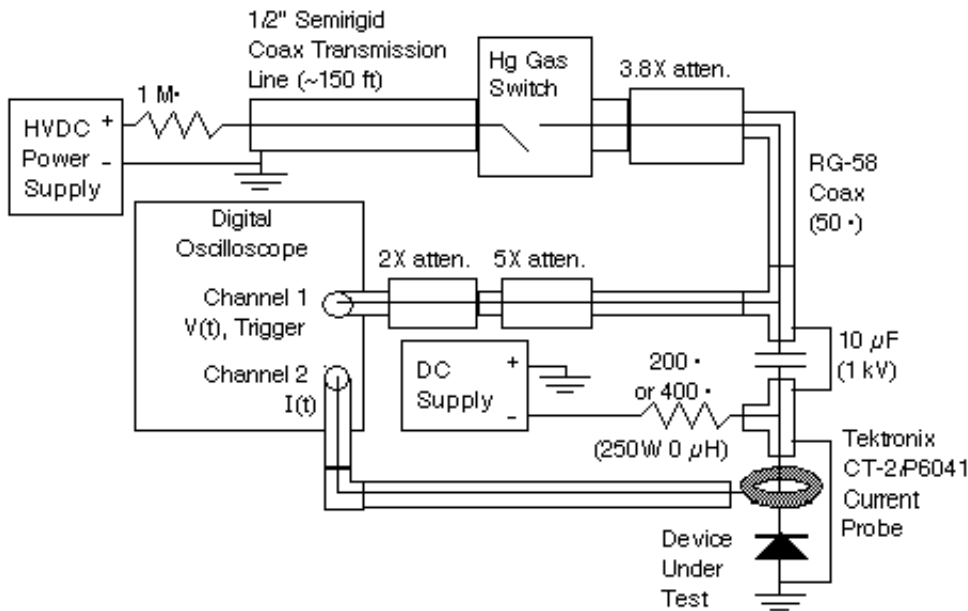


Fig. 3. Fast-risetime pulse-test circuit employed to measure p^+n diode reverse recovery. The fast-risetime pulse is formed by the discharge of the semirigid coax when the mercury vapor switch is momentarily triggered. The diode is initially forward biased by the DC supply through the 200 ohm (or 400 ohm) resistor. The 10 μ F high-voltage capacitor isolates the initial DC bias from the transmission line circuit, but permits the fast-risetime pulse to pass to rapidly switch the diode under test from forward bias into reverse bias. The Tektronix CT2/P6041 current probe/transformer monitors the transient reverse recovery current of the diode over the frequency range from 1 kHz to 500 MHz.

Experimentally recorded reverse recovery current transients from a 4H-SiC diode ($A = 8.1 \times 10^{-3} \text{ cm}^2$) for varying values of I_F and I_R are shown in Figures 4 and 5. Circuit parasitics (such as stray inductance, transmission-line delay and reflection, etc.) are believed responsible for some non-idealities in the recovery current waveform, such as a several nanosecond risetime and slightly non-constant I_R during the storage phase. The recovery of the measured current signal $I(t)$ towards $-I_F$ (instead of zero) at the end of the transients is an artifact of DC bias current energy stored in the current probe/transformer, so that $I(t)$ does not accurately represent the diode's reverse recovery current once inductively stored energy is released by the current probe/transformer as the magnitude of the diode recovery current decays to $-I_F$ somewhat after time t_s . Nevertheless, a relatively constant current storage phase regime ($0 < t < t_s$) is readily discernible from a strongly decaying recovery phase portion ($t > t_s$) of each current transient in Figures 4 and 5, thereby enabling reasonably accurate determination of t_s for each switching transient.

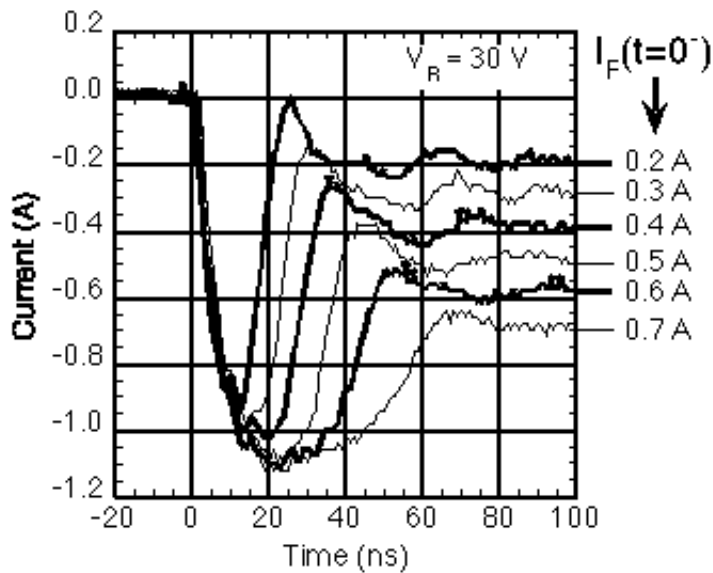


Fig. 4. Reverse recovery current transients recorded on $8.1 \times 10^{-3} \text{ cm}^2$ 4H-SiC diode as a function of varying initial forward bias. I_R is held approximately constant ($\sim 1 \text{ A}$) by fixing the reverse bias pulse amplitude while I_F is varied. The storage time increases as I_F is increases, consistent with classical silicon p^+n diode behavior and the fact that it takes longer for the increasing number of minority carriers injected at higher levels of I_F to recombine.

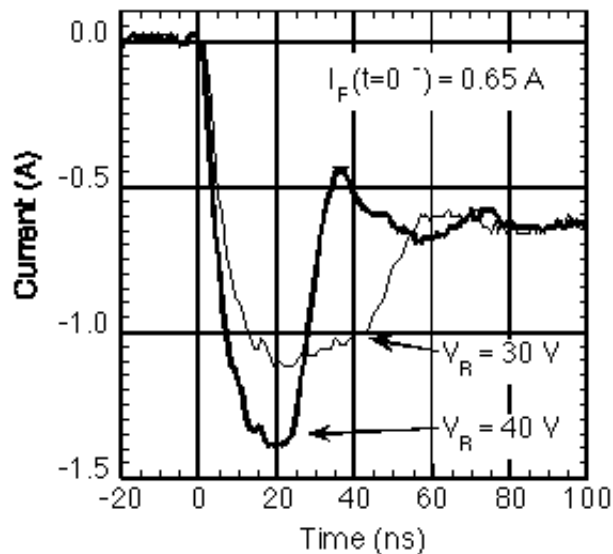


Fig. 5. Reverse recovery current transients recorded on $8.1 \times 10^{-3} \text{ cm}^2$ 4H-SiC diode as a function of varying reverse bias. Initial forward bias I_F is held constant at 0.65 A while the reverse bias pulse amplitude is changed from 30 V to 40 V . The storage time decreases as I_R increases, consistent with classical silicon p^+n diode behavior and the fact that higher I_R leads to quicker removal of excess holes.

As has been the case for silicon diode testing, storage times of well-behaved SiC p^+n junctions measured under varying I_F and I_R biasing conditions should follow relation (1). In Fig. 4, I_R is held almost constant by fixing the reverse bias pulse amplitude (accomplished by fixing the HVDC supply voltage) while I_F is varied by changing the DC forward bias supply voltage. The storage time increases as I_F is increased, consistent with relation (1) and the fact that it takes longer for the increasing number of minority carriers injected at higher levels of I_F to recombine. Fig. 5 shows the general effect of holding I_F constant while varying I_R (i.e., V_R) as the reverse bias pulse amplitude is changed from 30 V to 40 V. This behavior is again consistent with classical silicon diode behavior and relation (1), as increased I_R permits quicker diffusion current removal of excess holes during the switching transient leading to a decrease in t_s .

Quantitative agreement of storage time data with relation (1) can be checked by plotting t_s vs. I_R/I_F for any given diode. Fig. 6 shows experimental t_s vs. I_R/I_F data taken from switching transient measurements of two 4H-SiC p^+n devices from the same wafer. Also shown in Fig. 6 are theoretical fits of relation (1) to the measured storage time data for both devices, based on apparent minority carrier (hole) lifetimes of $\tau_p = 300$ ns and $\tau_p = 80$ ns for the larger and smaller devices, respectively. As expected, the experimental dependence of SiC p^+n diode storage time on I_R/I_F ratio shows good agreement with p^+n diode storage time theory.

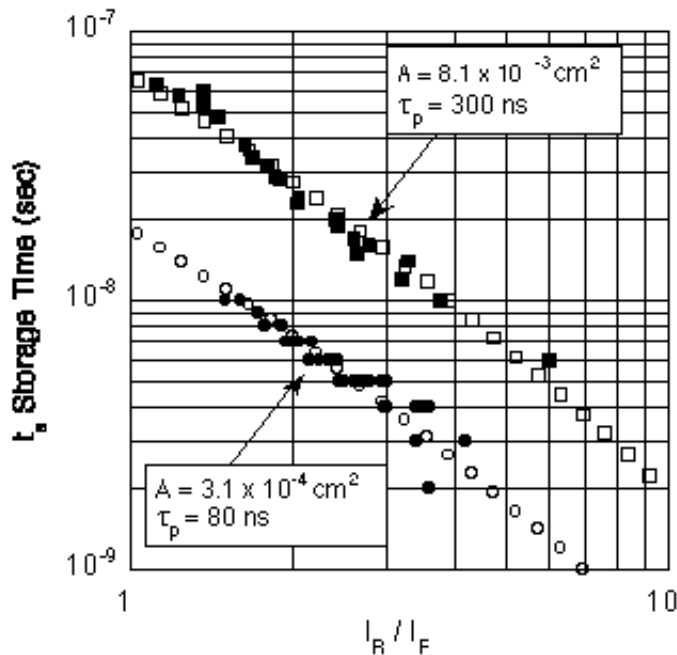


Fig. 6. Experimental variation of storage time t_s as a function of I_R/I_F ratio for two 4H-SiC p^+n diodes taken from the same wafer (filled symbols). Open symbols are plots of relation (1) calculated using τ_p that best fits experimental data from each device. Large decrease in τ_p with decreasing device size suggests perimeter recombination plays a

large role in limiting effective device minority carrier lifetime.

The large difference ($> 3 \times$) in measured hole lifetimes between two diodes on the same wafer indicates that physical mechanisms other than bulk Shockley - Read - Hall (SRH) recombination (i.e., recombination occurring at uniformly distributed recombination centers inherent to the bulk n-type SiC epilayer) are governing the effective minority carrier lifetime of these devices¹². It is well documented in the literature that when average minority carrier recombination/generation lifetimes decrease with decreasing device size, the physical mechanism of SRH perimeter surface recombination/generation occurring around the device periphery is often responsible^{13, 14}. Therefore, the average minority carrier (hole) lifetime τ_p measured and discussed up to this point is not necessarily the bulk carrier lifetime inherent to the SiC epilayer, but is more accurately viewed as an average (or effective) minority carrier lifetime ($\tau_{p \text{ Eff.}}$) that reflects SRH recombination occurring both in the bulk and around the surface periphery of a particular device.

Relation (1) is derived via one-dimensional analysis of minority carrier diffusion and recombination in a pn junction, where τ_p physically represents a uniform bulk minority carrier lifetime on the n-side of the junction². However in diodes where surface recombination is significant in addition to bulk recombination, lateral nonuniformities in the transient recovery process arise which necessitate a more complex two-dimensional analysis. A rigorous analysis of the two-dimensional recovery process was not undertaken as part of this work. Experimentally measured recovery transients were generally consistent with recovery transients predicted by one-dimensional theory. Therefore for purposes of initially estimating the relative importance of bulk and surface recombination, it is sufficient to express τ_p in relation (1) as a geometrically dependent $\tau_{p \text{ Eff.}}$ and study its experimental variation as a function of device geometry.

An approximation for $\tau_{p \text{ Eff.}}$ expressed in terms of device geometry, bulk material recombination lifetime, and surface recombination rate (velocity) can be derived as follows. The total bulk and perimeter SRH recombination occurring within a p^+n diode of area A and perimeter P can be expressed as:

$$R_{\text{Eff.}}A = R_{\text{Bulk}}A + R_{\text{Perim.}}P \quad (2)$$

where $R_{\text{Eff.}}$ is the effective (or average) recombination rate of the device, R_{Bulk} is the area-normalized bulk minority carrier recombination rate ($\text{cm}^{-3}\text{sec}^{-1}$) inherent to the n-side of the semiconductor p^+n junction, and $R_{\text{Perim.}}$ is the perimeter normalized minority carrier recombination rate ($\text{cm}^{-2}\text{sec}^{-1}$) associated with surface recombination around the diode junction periphery. Using commonly employed simplifications of SRH theory^{12, 14}, relation (2) can be rewritten in terms of excess minority carrier concentration on the n-side of the

junction Δp_n , bulk minority carrier lifetime inherent to the bulk semiconductor on the n-side of the junction $\tau_{p \text{ Bulk}}$, and an effective hole surface recombination velocity $s_{p \text{ Perim.}}$ of the n-type semiconductor surface near the metallurgical pn junction:

$$\frac{\Delta p_n}{\tau_{p \text{ Eff.}}} A \approx \frac{\Delta p_n}{\tau_{p \text{ Bulk}}} A + s_{p \text{ Perim.}} \Delta p_n P \quad (3)$$

Because devices on the same wafer are subjected to identical material growth and device processing, we assume that $s_{p \text{ Perim.}}$ and $\tau_{p \text{ Bulk}}$ do not vary significantly from device to device. By dividing both sides of (3) by $\Delta p_n A$ one arrives at a simple linear expression that relates bulk minority carrier lifetime and surface recombination velocity to the effective (or average) minority carrier lifetime of the device:

$$\frac{1}{\tau_{p \text{ Eff.}}} \approx \frac{1}{\tau_{p \text{ Bulk}}} + s_{p \text{ Perim.}} \left(\frac{P}{A} \right) \quad (4)$$

Relation 4 predicts that $1/\tau_{p \text{ Eff.}}$ (i.e., the measured value of $1/\tau_p$) will vary linearly as a function of perimeter-to-area ratio (P/A) as the device size changes. Fig. 7 shows a plot of $1/\tau_p$ vs. P/A constructed from reverse-recovery data of various same-wafer 4H-SiC diodes measured in this work. The Fig. 7 data follows a linear trend consistent with relation (4), so that $\tau_{p \text{ Bulk}}$ and $s_{p \text{ Perim.}}$ can be calculated from the y-intercept and slope of the best fit line, respectively. The inverse y-intercept of Fig. 7 yields an apparent bulk hole lifetime $\tau_{p \text{ Bulk}}$ inherent to the 4H-SiC n-type epilayer of $0.7 \mu\text{s}$, while the slope corresponds to an effective surface recombination velocity $s_{p \text{ Perim.}}$ of approximately $5 \times 10^4 \text{ cm/sec}$.

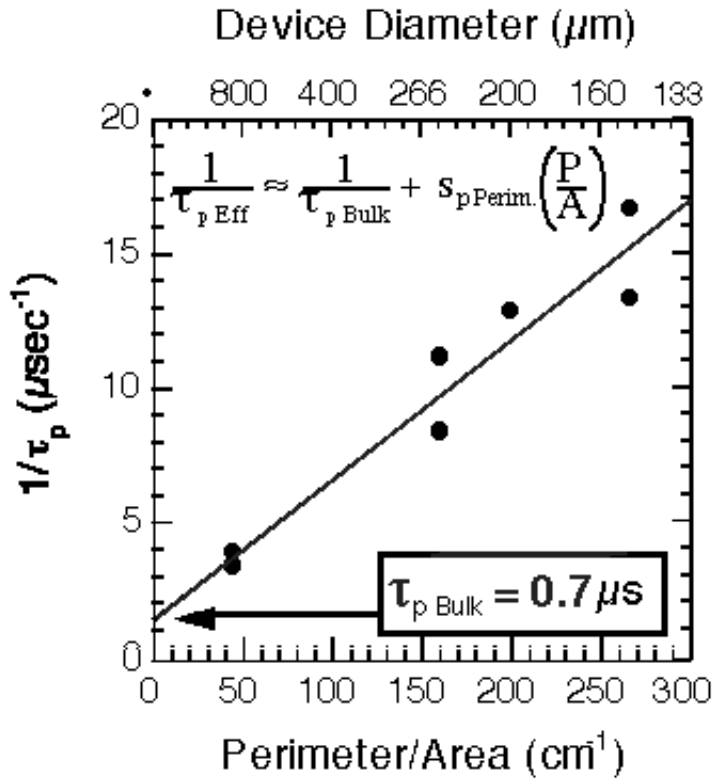


Fig. 7. Inverse effective device minority carrier lifetime (τ_p) versus perimeter-to-area ratio (P/A) for packaged 4H-SiC p^+n diodes that underwent reverse recovery transient testing and analysis. The strong slope in this plot indicates that surface recombination around the etched diode perimeter dominates the effective minority carrier lifetime of the device, instead of recombination occurring in the bulk SiC material itself. The inverse y-intercept of Fig. 7 yields a bulk hole lifetime $\tau_{p \text{ Bulk}}$ inherent to the 4H-SiC n-type epilayer of $0.7 \mu\text{s}$, while the slope corresponds to an effective surface recombination velocity $s_{p \text{ Perim}}$ of approximately $5 \times 10^4 \text{ cm/sec}$.

It is apparent from the strong slope of Fig. 7 that perimeter surface recombination strongly influences the electrical switching performance of these 4H-SiC rectifiers. As device size shrinks to $1.77 \times 10^{-4} \text{ cm}^2$ (150 μm diameter), surface recombination drops the average device recombination lifetime to 60 ns, more than a factor of 10 smaller than the bulk hole lifetime inherent to the SiC n-type epilayer. Even the longest average carrier lifetime of $0.3 \mu\text{s}$ measured on the largest device ($8.1 \times 10^{-3} \text{ cm}^2$) is less than half $\tau_{p \text{ Bulk}}$. Therefore, the bulk minority carrier lifetime had little impact on the overall switching performance of these devices.

The strong experimental dependence of τ_p on device geometry clearly indicates that a significant percentage carriers initially injected near the center of the devices must be recombining at the diode periphery. This is perhaps somewhat unexpected due to the fact that hole diffusion lengths of comparably-doped 4H-SiC reported in the literature¹⁵ or calculated

via the Einstein relation¹² are much shorter (under 20 μm) than the 75 μm to 450 μm radial device dimensions studied in this work.

It is surmised that drift arising from self-induced fields plays a key role in the lateral transport of holes to the device periphery, similar to the manner in which self-induced fields are responsible for most lateral charge transfer in long-channel Charge Coupled Devices (CCD's)^{16,17}. At $t=0^+$ before substantial bulk recombination occurs in the diode the large hole charge leftover from high injection is analogous to a CCD charge packet. Given sufficient charge densities, self-induced electric field drift transport will strongly and rapidly redistribute holes towards the diode edges similar to what Carnes et. al.¹⁷ determined in their silicon CCD investigations. Furthermore, the enhanced recombination at the diode perimeter serves to remove holes from the edge of the device, performing a similar carrier removal function as an adjacent pull-clocked CCD cell. Proper numerical verification of this speculative model will require rigorous two-dimensional transient analysis of the reverse recovery process. While beyond the immediate scope of this experimental work, it is hoped that future two-dimensional analysis efforts will further more detailed understanding of the reverse recovery behavior observed in these 4H-SiC diodes.

When silicon diodes are operated at sufficiently high injection forward bias, bulk Auger recombination has been shown to decrease average minority carrier lifetime, so that τ_p actually drops as J_F is further increased^{4, 18}. There was no observable trend in t_s as a function of either J_F or J_R to suggest that bulk Auger recombination played any significant role in this work. Direct comparison of t_s measured in different-sized devices at $J_F \cong 1000 \text{ A/cm}^2$ and $J_R \cong 2000 \text{ A/cm}^2$ revealed behavior consistent with Fig. 7, in that smaller devices exhibited significantly shorter storage times than larger devices. This behavior supports the hypothesis that perimeter-governed SRH surface recombination, not bulk Auger recombination, is the major mechanism responsible for degradation of average device minority carrier lifetime.

Discussion

The abovementioned observations underscore the importance of studying device electrical performance as a function of device perimeter-to-area ratio. If, for example, only 150 μm diameter devices had been measured in this work, it would have been easy to draw the mistaken conclusion that the bulk minority carrier lifetime of the n-type 4H-SiC epilayer was around 60 ns, which is more than a factor of 10 smaller than the actual bulk lifetime obtained by properly accounting for perimeter recombination effects. It is often overlooked that factors other than bulk material properties can govern electrical device minority carrier recombination/generation lifetime. This expedient oversight seems commonplace in the SiC literature, as bulk material quality is often blamed out of hand for sub-par experimental SiC bipolar device performance.

By example, this work raises the possibility that perimeter recombination effects may be

responsible for poor effective minority carrier lifetimes and limited performance obtained in many SiC bipolar junction devices. Almost all scientific literature documenting experimental SiC bipolar diodes and transistors has neglected to report electrical performance as a function of perimeter-to-area ratio. The degree to which perimeter recombination plays a role in limiting device effective minority carrier lifetime is naturally expected to vary from experiment to experiment, as each different SiC bipolar process will likely have its own bulk and surface recombination properties. For example, epitaxially doped SiC layers will likely have different bulk recombination/generation lifetimes than layers doped by ion-implantation, and polytype and doping density have also been optically shown to affect $\tau_{p \text{ Bulk}}$.^{6, 19} Surface preparation techniques such as oxidation and face-polarity (C-face vs. Si-face) should also influence SiC surface recombination/generation velocity, similar to what was observed for generation velocity in prototype 6H-SiC pn junction nonvolatile random access memory cells²⁰. Improved surface passivation technologies to reduce surface recombination velocity and improve bipolar device performance have been successfully employed in other semiconductor material systems²¹. This suggests that similar significant improvements to SiC bipolar device performance may be possible once more optimized SiC surface passivation approaches have been developed.

While keeping in mind important experimental differences, it is useful to compare trends observed in this study with previously reported SiC data. A prior study of 6H-SiC diode I-V characteristics did not directly measure minority carrier lifetime²². Nevertheless, the behavior of forward current density as a function of P/A ratio was found to be entirely dominated by perimeter surface recombination, as there was no observable bulk contribution to measured recombination currents in the exponential $n = 2$ region of the I-V characteristics. Because micropipes limit SiC device sizes, the P/A ratios of previously reported bipolar devices is similar to or higher than the P/A ratios of our diodes whose average hole lifetime was dominated by perimeter surface recombination. Commonly employed multi-fingered or multi-cell device designs (as in Ref. 5 for example) will have even larger P/A ratios, which will even further elevate the role of surface recombination on bipolar device electrical properties. Photoluminescence decay measurements have shown that minority carrier lifetimes in 6H-SiC n-type epilayers exhibit a strong dependence on doping, from 90 ns at $7 \times 10^{17} \text{ cm}^{-3}$ to 450 ns at $4 \times 10^{14} \text{ cm}^{-3}$.^{6, 23} A similarly-sized variation in average device minority carrier lifetime (60 ns to 300 ns) was observed in this study by changing the P/A ratio 44 cm^{-1} to 267 cm^{-1} . This suggests that perimeter recombination effects can influence SiC device minority carrier lifetime as strongly as doping and should therefore not be neglected in bipolar SiC device design and analysis. The $0.7 \mu\text{s}$ bulk hole lifetime in our $2 - 4 \times 10^{16} \text{ cm}^{-3}$ intentionally nitrogen-doped 4H-SiC epilayer appears consistent with lifetimes optically ascertained by Janzen et. al.^{6,19,23}, in that they observed shorter lifetimes in comparably-doped 6H-SiC epilayers while they measured longer lifetimes in lower-doped (unintentional low 10^{14} cm^{-3}) 4H-SiC epilayers.

Summary

This work measured minority carrier lifetimes in epitaxial 4H-SiC p⁺n junction rectifiers via analysis of diode reverse recovery switching characteristics. Perimeter surface recombination was determined as the primary mechanism limiting minority carrier lifetime, with bulk recombination inherent to the 4H-SiC n-epilayer playing almost no role in device reverse recovery characteristics. Now that the importance of perimeter recombination has been highlighted by this study, additional studies should further elucidate the impact of perimeter-governed lifetime on other implementations of SiC bipolar electronic devices. Moreover, the development of improved SiC junction termination and surface passivation technologies should be pursued in order to reduce undesired surface recombination effects on SiC bipolar lifetime and device performance.

Acknowledgments

This work was carried out by NASA Lewis Research Center under internal funding. The author would like to gratefully acknowledge the assistance provided by Christian Fazi of US Army Research Laboratory as well as David Larkin, J. Anthony Powell, Carl Salupo, Luann Keys, Andrew Trunek, John Heisler, Bruce Viergutz, Gene Schwarze, Jan Niedre, Glenn Beheim, and Lawrence Matus of NASA Lewis in carrying out this work.

References

- ¹ S. Nakashima, H. Matsunami, S. Yoshida, and H. Harima, eds., *Institute of Physics Conference Series, no. 142, Silicon Carbide and Related Materials 1995* (Bristol, UK: Institute of Physics, 1996).
- ² G. W. Neudeck, *The PN Junction Diode, vol. 2, 2nd. ed., Modular Series on Solid State Devices*, eds. G. W. Neudeck and R. F. Pierret (Reading, MA: Addison-Wesley, 1989).
- ³ G. W. Neudeck, *The Bipolar Junction Transistor, vol. 3, 2nd. ed., Modular Series on Solid State Devices*, eds. G. W. Neudeck and R. F. Pierret (Reading, MA: Addison-Wesley, 1989).
- ⁴ S. M. Sze, *Physics of Semiconductor Devices, 2nd. ed.* (New York: Wiley-Interscience, 1981), p. 61.
- ⁵ Y. Wang, W. Xie, J. A. Cooper, Jr., M. R. Melloch, and J. W. Palmour, *Institute of Physics Conference Series, no. 142, Silicon Carbide and Related Materials 1995*, eds. S. Nakashima, H. Matsunami, S. Yoshida, and H. Harima (Bristol, UK: Institute of Physics, 1996), p. 809.
- ⁶ E. Janzen and O. Kordina, *Institute of Physics Conference Series, no. 142, Silicon Carbide and Related Materials 1995*, eds. S. Nakashima, H. Matsunami, S. Yoshida, and H. Harima (Bristol, UK: Institute of Physics, 1996), p. 653.

- ⁷ K. Xie, J. H. Zhao, J. R. Flemish, T. Burke, W. R. Buchwald, G. Lorenzo, and H. Singh, *IEEE Electron Device Lett.* 17, 142 (1996).
- ⁸ O. Kordina, J. P. Bergman, A. Henry, E. Janzen, S. Savage, J. Andre, L. P. Ramberg, U. Lindefelt, W. Hermansson, and K. Bergman, *Appl. Phys. Lett.* 67, 1561 (1995).
- ⁹ Cree Research, Inc., 2810 Meridian Parkway, Suite 176, Durham, NC 27713.
- ¹⁰ D. J. Larkin, P. G. Neudeck, J. A. Powell, and L. G. Matus, *Appl. Phys. Lett.* 65, 1659 (1994).
- ¹¹ R. H. Kingston, *Proc. IRE* 42, 829 (1954).
- ¹² R. F. Pierret, *Advanced Semiconductor Fundamentals, vol. 6, Modular Series on Solid State Devices*, eds. G. W. Neudeck and R. F. Pierret (Reading, MA: Addison-Wesley, 1987).
- ¹³ C. H. Henry, R. A. Logan, and F. R. Merrit, *J. Appl. Phys.* 49, 3530 (1978).
- ¹⁴ P. E. Dodd, T. B. Stellwag, M. R. Melloch, and M. S. Lundstrom, *IEEE Trans. Electron Devices* 38, 1253 (1991).
- ¹⁵ R. Raghunathan and B. J. Baliga, "EBIC Measurements of Diffusion Lengths in Silicon Carbide," presented at Electronic Materials Conference, Santa Barbara, CA, June 1996, p. 18.
- ¹⁶ D. K. Schroder, *Advanced MOS Devices, vol. 7, Modular Series on Solid State Devices*, eds. G. W. Neudeck and R. F. Pierret (Reading, MA: Addison-Wesley, 1987), p. 77.
- ¹⁷ J. E. Carnes, W. F. Kosonocky, and E. G. Ramberg, *IEEE Trans. Electron Devices* 19, 798 (1972).
- ¹⁸ J. Krausse, *Solid-St. Electron.* 17, 427 (1974).
- ¹⁹ O. Kordina, J. P. Bergman, C. Hallin, and E. Janzen, *Appl. Phys. Lett.* 69, 679 (1996).
- ²⁰ Y. Wang, J. A. Cooper, Jr., M. R. Melloch, S. T. Sheppard, J. W. Palmour, and L. A. Lipkin, *J. Electron. Mater.* 25, 899 (1996).
- ²¹ C. J. Sandroff, R. N. Nottenburg, J. C. Bischoff, and R. Bhat, *Appl. Phys. Lett.* 51, 439 (1987).
- ²² P. G. Neudeck, D. J. Larkin, J. E. Starr, J. A. Powell, C. S. Salupo, and L. G. Matus, "Electrical Characterization of 3C- and 6H-SiC PN Junction Diodes Grown by CVD on Low-Tilt-Angle 6H-SiC Wafers," presented at Workshop on SiC Materials and Devices,

Charlottesville, VA, (1992), p. 39.

²³ O. Kordina, J. P. Bergman, A. Henry, and E. Janzen, *Appl. Phys. Lett.* 66, 189 (1995).